Materials Research Bulletin 44 (2009) 600–605

Contents lists available at ScienceDirect

Materials Research Bulletin

journal homepage: www.elsevier.com/locate/matresbu

Photoluminescence characteristics of ZnO clusters confined in the micropores of zeolite L

Fang Wang [a,b], Hongwei Song [c,*], Guohui Pan [a,b], Libo Fan [a,b], Qilin Dai [a,b], Biao Dong [a,b], Huihui Liu [a,b], Jihong Yu [d], Xi Wang [d], Li Li [d]

[a] Key Laboratory of Excited State Physics, Changchun Institute of Optics, Fine Mechanics and Physics, Chinese Academy of Sciences, 16 Eastern South-Lake Road, Changchun 130033, People's Republic of China
[b] Graduate School of Chinese Academy of Sciences, Beijing 100039, People's Republic of China
[c] State Key Laboratory of Integrated Optoelectronics, College of Electronic Science and Engineering, JiLin University, Changchun 130012, People's Republic of China
[d] State Key Laboratory of Inorganic Synthesis and Preparative Chemistry, College of Chemistry, Jilin University, Changchun 130012, People's Republic of China

ARTICLE INFO

Article history:
Received 8 February 2008
Received in revised form 8 June 2008
Accepted 6 July 2008
Available online 15 July 2008

Keywords:
A. Composites
A. Semiconductors
D. Optical properties

ABSTRACT

Sub-nanometric ZnO clusters were prepared in the micropores of zeolite L by the incipient wetness impregnation method. The X-ray patterns (XRD), transmission electron microscope (TEM), N_2 adsorption–desorption isotherms, UV–vis absorption spectra (UV–vis) and photoluminescence spectra (PL) were used to characterize the composite materials. The results indicate that a small amount of sub-nanometric ZnO clusters can be introduced into the channel of zeolite L, however, when the amount of ZnO loading exceeds 20 wt%, macrocrystalline ZnO appears on the external surface of zeolite L. Different from bulk ZnO materials, these sub-nanometric ZnO clusters exhibit their absorption onset below 255 nm and a blue luminescence band in the range of 404–422 nm. The temperature-dependent luminescence demonstrates that the amount of the ZnO loading significantly affects the exciton–phonon interaction between the ZnO clusters and the zeolite host. The ZnO clusters exhibit a picosecond scale emission lifetime at room temperature.

1. Introduction

Wide band semiconductors have been the focus of modern research due to their potential applications in many areas, such as catalysis [1], optical sensitizers, photocatalysts [2], light converting electrodes [3], laser diodes and high-speed electronic devices, etc. Among all semiconductors, ZnO has attracted considerable attention due to its wide band gap (3.37 eV) [4] and large exciton binding energy (60 meV) [5–7]. Typical applications of ZnO include sensors, ultraviolet (UV) light-emitting devices, solar cells, transducers, etc. As we know, as the particle sizes of semiconductors decrease to nanometer scales, their optical properties can be tuned due to the quantum size effect (QSE) [8–9]. When the particle size of ZnO decreases to nanometer and even sub-nanometer scale, the material usually exhibits strong QSE, taking on different properties from bulk material [10–12]. Until now, much of research has been emphasized on nanometer or micrometer ZnO material; however, only little attention has been paid to the sub-nanometric ZnO clusters. Because ZnO clusters are so small and unstable, many materials, such as colloidal [13], porous glasses [14], certain polymers [15] and zeolites are used as hosts or stabilizers for the preparation of ZnO clusters. Among them, the microporous zeolites can provide well-ordered pores, stable and antacid environment to encapsulate ZnO clusters. At the same time, the size of ZnO clusters can be tailored by microporous zeolite. By incipient wetness impregnation method, Chen et al. [16] prepared different amounts of ZnO clusters in the pores of HZSM-5 (MFI type) and HY (FAU type), which had the three-dimensional pore structure, respectively. They also studied the optical properties of ZnO clusters confined in zeolite and observed blue photoluminescence at room temperature.

In the present paper, a host of microporous aluminosilicate zeolite L (Linde Type L) was used to encapsulate ZnO clusters, which possesses smaller channel diameter (7–8 Å) than those of mesoporous molecular sieves and one dimensionality in framework. The framework of the zeolite possesses much higher stability in treatment at high temperature under hydrothermal condition and in acidic media. It is easier to encapsulate ZnO clusters. Compared with previous results [16], the absorption edge and the blue emission band both blue-shift further due to stronger QSE.

* Corresponding author. Fax: +86 431 86176320.
E-mail address: hwsong2005@yahoo.com.cn (H. Song).

0025-5408/$ – see front matter © 2008 Elsevier Ltd. All rights reserved.
doi:10.1016/j.materresbull.2008.07.002

And more, the dynamics and temperature-dependent photoluminescence were systemically studied to better understand the optical properties of ZnO clusters.

2. Experimental

2.1. Synthesis

Zeolite L (SiO_2/Al_2O_3 = 6.5) was provided by China University of Petroleum Beijing. The zeolite L is hexagonal (space group *P*6/*mmm*) in crystal structure, whose framework is composed of cancrinite cages (CAN-cages) and double six-rings (D6Rs). The linking of CAN-cages and D6Rs in [011] direction leads to the formation of CAN-D6R-CAN cage columns. These six cage columns connect with each other, surrounding the *c*-axis and building up 12-membered rings with a 7.1 Å free diameter, which is schematically illustrated in Fig. 1 [17].

For the preparation of ZnO clusters, typically, an appropriate volume of $Zn(CH_3CHOO)_2{\cdot}2H_2O$ aqueous solution was added into 100 mg of zeolite powder L with continuous stirring. This mixture was stirred for 24 h in a hot water bath until dried. The ZnO/L composite was then obtained after a further dry at 80 °C for overnight and subsequent annealing at 550 °C for 5 h. The composites of different ZnO loadings were obtained by adjusting the concentration of $Zn(CH_3CHOO)_2{\cdot}2H_2O$ aqueous solution. The weight ratios of $Zn(CH_3CHOO)_2{\cdot}2H_2O$ to zeolite L for the samples a, b, c, d, e were 5:1, 10:1, 20:1, 25:1, 30:1, respectively.

2.2. Measurements

All the samples were characterized by XRD using a Siemens D5005 diffractometer with Cu Kα radiation (λ = 1.5418 Å). The morphologies and electron diffraction of the samples L and ZnO/L were characterized by a JEM-3010 transmission electron microscope (TEM) with an accelerating voltage of 200 kV. N_2 adsorption/desorption isotherms were recorded using a micromeritics Gemini V2380 instrument (the samples were outgassed under vacuum at 170 °C for 1 h.) and N_2 was used as the analysis gas at 77 K. Specific surface area and micropore volume are calculated with Langmuir mode and *t*-plot (DeBoer) method, respectively [18]. The UV–vis absorption spectra were recorded at a UV–vis–NIR scanning spectrophotometer (SHIMADZU).

In the measurement of the photoluminescence spectra, a 266 nm light generated from the fourth-harmonic-generator pumped by the pulsed Nd:YAG laser was used as excitation source, with pulse duration of 10 ns, and repetition frequency of 10 Hz. Photoluminescence spectra were measured by the LabRaman Spectrometer under the excitation of a 325 nm He–Cd laser source. In the measurements of the temperature dependence of PL, the samples were put into a cryogenic unit cooled by liquid nitrogen, in which the temperature varied from 77 K to room temperature. Fluorescent dynamics were measured on an FL920-Fluorescence Lifetime Spectrometer (Edinburgh Instruments) with MCP-PMT. The excitation source was an optical parametric amplifier (Spectra Physic Co. Ltd.), which provided a 130 fs full width at half maximum (FWHM) pulse (wavelength of 345 nm, repetition rate of 1 kHz).

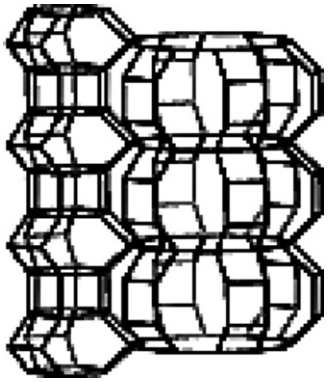

Fig. 1. Schematic diagrams of the framework structures for zeolite L.

3. Results and discussion

3.1. Characterization

Firstly, the physisorption method was adopted to analyze the texture properties of ZnO/L with different ZnO loadings. The information on the pore texture of ZnO/L is helpful to understand the status of ZnO clusters encapsulated in the hosts. The langmuir area and *t*-plot volume of the samples are listed in Table 1. In comparison to the zeolite L, the langmuir area and *t*-plot volume of the ZnO/L (5 wt%) composites significantly decrease. As the ZnO loading increases further, the langmuir area and the *t*-plot volume decrease gradually but slowly. The above results suggest that (1) the pores of the zeolites are partly filled, and the fillings should be ZnO clusters in term of the chemical reaction in the preparation processes; (2) as the ZnO loadings increase from 5 to 30 wt%, ZnO clusters encapsulated into the pores of the zeolites increase only a little. In other words, not all of the ZnO loadings can be encapsulated into the pores of the zeolites if the amount of the ZnO loadings is excessive.

To identify the above conclusions further, the TEM images of different samples were taken and shown in Fig. 2. It can be seen from Fig. 2(a) that paralleled and homogeneous pores are formed in the zeolite L. The average pore diameter of zeolite L is about 7.1 Å, which is well consistent with the theoretical result. As seen in Fig. 2(b), there are some dark regions on the photograph besides the paralleled pores, which are the ZnO inclusions in the ZnO/L (5 wt%) composite. According to the above physisorption results, this clearly indicates that the pores are partially filled with ZnO clusters. Concerning the cell parameters of ZnO (*a* = 3.2396 Å, *c* = 5.2065 Å) and the pore diameter (7.1 Å) of zeolite L, the present ZnO cluster should subject to considerable lattice distortion when confined into zeolite L. The ZnO clusters may contain tens of molecules and be of Angstrom order of magnitude in size. Besides ZnO clusters encapsulated into the pores, some ZnO nanoparticles ranging from several nanometers to ten nanometers cover the extra surface of zeolite L (see Fig. 2(c)). The selective area electron diffraction (SAED) pattern (see Fig. 2(d)) was taken on ZnO clusters inside the zeolite (5 wt% ZnO/L composite), which indicates that it is polycrystalline. Note that macrocrystalline ZnO can also be observed when ZnO loading is more than 20 wt%.

Fig. 3 shows the XRD patterns of the ZnO/L composites with different ZnO loadings in contrast to the zeolite L. In the zeolite L, a

Table 1
Langmuir surface area and *t*-plot micropore volume of the ZnO/L composites with different ZnO loadings

ZnO/L with different ZnO loading (wt%)	Langmuir surface area (m^2/g)	*t*-Plot micropore volume (cm^3/g)
0	118.6300	0.01156
5	65.1754	0.00273
10	63.2969	0.00265
20	50.3523	0.00194
25	48.9173	0.00176
30	46.7934	0.00155

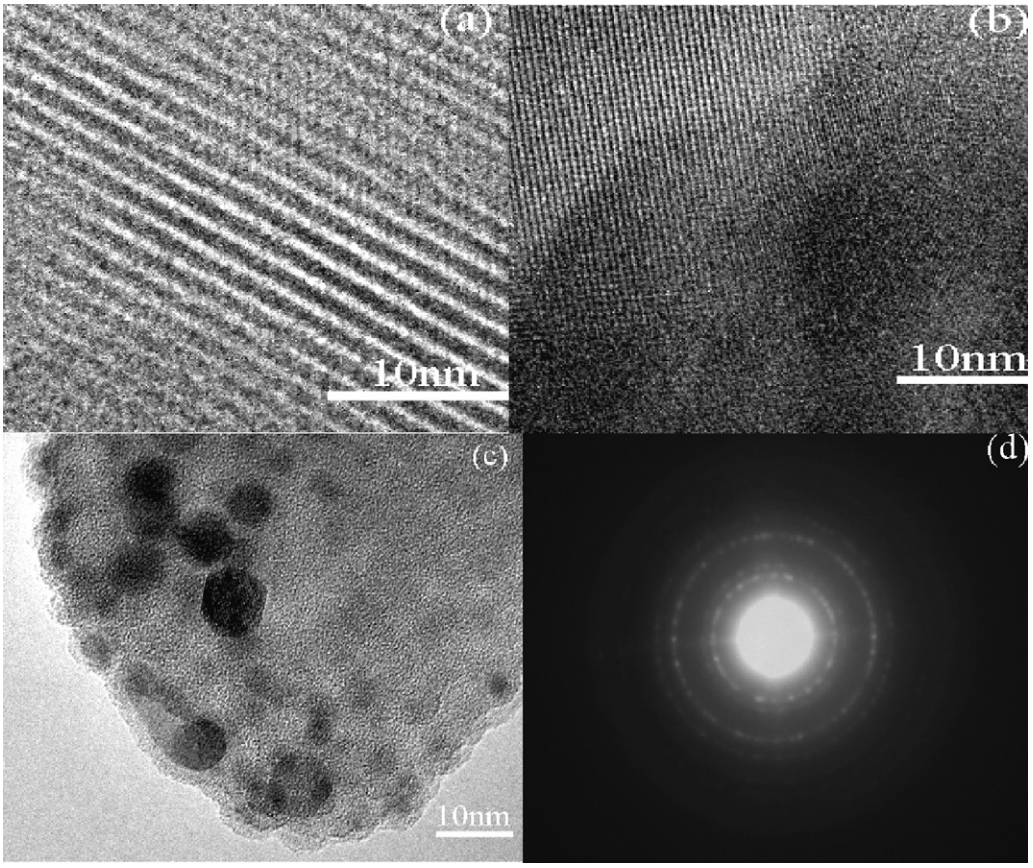

Fig. 2. TEM pictures of zeolite L (a), 5 wt% ZnO loading (b), 30 wt% ZnO loading (c) and the electron diffraction of 5 wt% ZnO/L composite (d).

number of diffraction peaks appear in the range of $2\theta = 5–40^\circ$ due to the crystalline structure of the zeolite L. In the ZnO/L composites, the same diffraction peaks could be clearly observed. No peak caused by crystalline ZnO could be observed as the ZnO loading is less than 20 wt%. As the ZnO loading exceeds 20 wt%, the diffraction peaks caused by hexagonal ZnO appear at $2\theta = 31.78^\circ$, 34.44° and 36.25°, corresponding to the planes of (1 0 0), (0 0 2), and (1 0 1), respectively. Like what we could see from the TEM images, as the ZnO loading is less than 20 wt%, only ZnO clusters as well as small ZnO nanoparticles are formed. Therefore, the invisibility of the ZnO diffraction peaks further indicates that ZnO clusters and the nanoparticles form inside the pore of zeolite and on the surface of the zeolite, respectively. [19–20]. The crystalline ZnO appearing in the XRD patterns are mainly caused by macrocrystalline ZnO formed on the surface of zeolite L.

Fig. 4 shows the UV–vis absorption spectra of the ZnO/L composites with different ZnO loadings. In the zeolite L, a weak band appears around 227 nm, which is assigned to the host absorption of the zeolite. When the ZnO loading is less than 10 wt% in the composites, two absorption bands appear, locating around

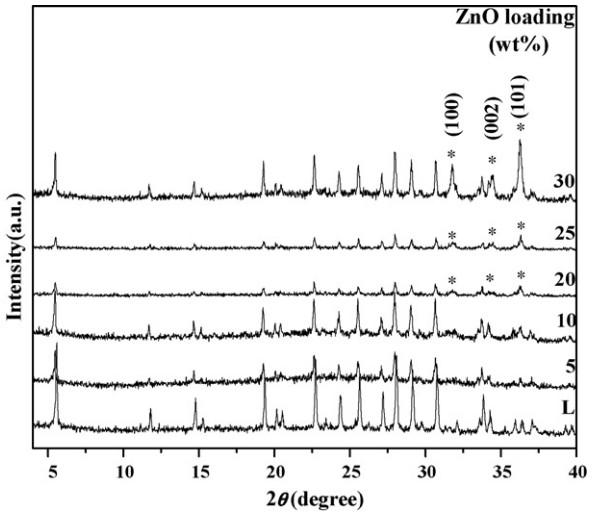

Fig. 3. XRD patterns of ZnO/L with different ZnO loadings. The asterisks denote the diffraction peaks of ZnO crystal with hexagonal structure.

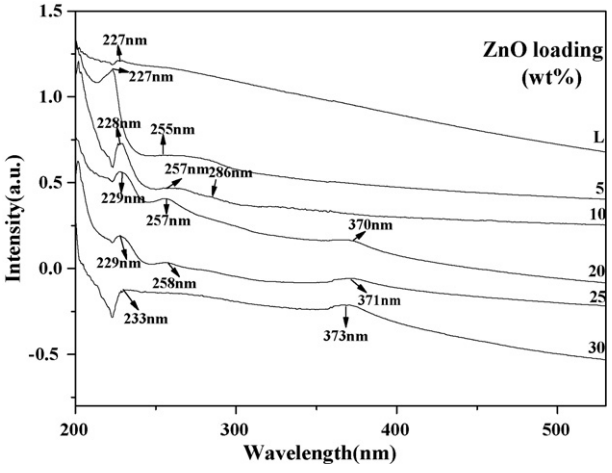

Fig. 4. UV–vis absorption spectra of ZnO/L with different ZnO loadings.

227 and 255 nm, which correspond to the host absorption of zeolite and ZnO clusters confined in the pores of zeolite L, respectively. In contrast, the host absorption band of zeolite L becomes much stronger, which could be attributed to the interaction between the zeolite and ZnO clusters. In the light of Brus model [8,21], the dependence of the shift of the band gap value on the particle radius can be given by

$$E = E_g^{bulk} + \frac{\hbar^2\pi^2}{2r^2}\left(\frac{1}{m_e} + \frac{1}{m_h}\right) - 1.8\frac{e^2}{kr} \quad (1)$$

where E_g^{bulk} is the band gap of bulk ZnO, r is the particle radius, m_e is the effective mass of an electron, m_h is the effective mass of a hole, k is the dielectric constant of semiconductor and $k = 3.7$, $\hbar$ is Planck's constant and e is the charge on the electron. Based on Eq. (1), the diameter for ZnO clusters corresponding to 255 nm adsorption is deduced to be $2r = 0.62$ nm. The result indicates that ZnO clusters, having an optical absorption with onset wavelength at about 255 nm, are formed in the pores of zeolite L for low ZnO loading. With increasing ZnO loading, the bands around 227 and 255 nm both shift to the red. At the same time, a shoulder gradually appears in the red side of the 255 nm peak, locating around 286 nm. This shoulder is attributed to the adsorption of nanocrystalline ZnO on the surface of the zeolite. According to Eq. (1), the nanocrystal is about 1.5 nm in diameter. When the ZnO loading exceeds 20 wt%, a band around 370 nm also appears, which corresponds to a critical threshold of macrocrystalline ZnO. The above TEM and UV–vis absorption experiments show that the 20 wt% loading is a critical threshold of ZnO dispersion on zeolite L. When ZnO loading is less than the critical threshold, ZnO cluster is dispersed into the pores of zeolite L. In addition, some ZnO nanocrystals were also formed on the surface of the zeolite. The excessive ZnO is distributed in macrocrystalline form on the external surface of the zeolite L.

3.2. Photoluminescence spectra

On the basis of the UV–vis absorption spectra, 266 and 325 nm lasers were selected as excitation sources to study the luminescence characteristics of the ZnO/L composites. The excitation wavelength of 266 nm locates in the absorption band (250–300 nm) of ZnO clusters confined in zeolites as well as nanoparticles related to different defect centers, whereas the excitation wavelength of 325 nm is inside the absorption band of ZnO clusters, nanocrystals ZnO and macrocrystalline ZnO. Therefore, the spectra excited by 266 nm can give the information mainly about ZnO clusters inside of zeolites as well as nanocrystals ZnO on the surface of the zeolites. The spectra excited by 325 nm can present the information about ZnO cluster inside of zeolites, nanocrystals ZnO and macrocrystalline ZnO outside of zeolite.

Fig. 5 shows the spectra of ZnO/L with different ZnO loadings under the excitation of 266 nm. Since the zeolite L is composed of SiO_2 and Al_2O_3 ($SiO_2/Al_2O_3 = 6.5$), there exist at least two kinds of chemical bonds in the zeolite network, more Si–O–Si and fewer Si–O–Al. Herein the broad emission band centered at 346 nm in the zeolite L was ascribed to the host emission related to Si–O–Si in the zeolite L given the fact that its photoluminescence usually ranges from 300 to 550 nm [22]. In the 5 wt% ZnO/L sample, besides the weak emission band originating from the zeolite L, a blue emission band peaking at 404 nm also appears which should correspond to ZnO clusters confined in the pores of zeolite L. With increasing ZnO loadings, the blue band becomes stronger and the emission spectra can be decomposed into two components, A and B, centering at 408 nm and 503 nm, respectively. In contrast, the emission intensity of the peak B (green) increases with increasing ZnO

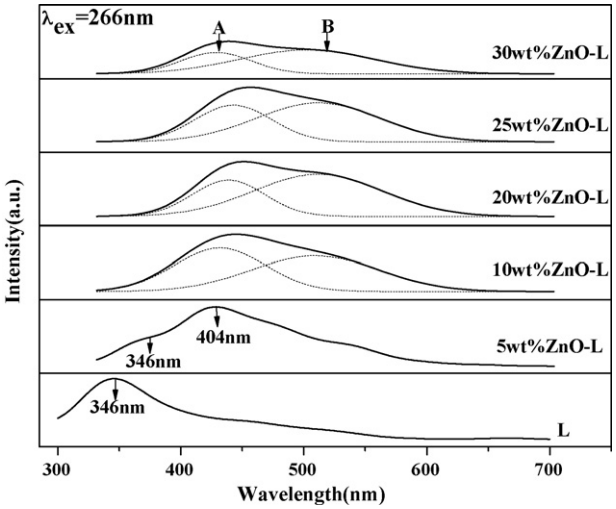

Fig. 5. Emission spectra of ZnO/L with different ZnO loadings ($\lambda_{ex} = 266$ nm).

loadings. Combined with the results of UV–vis absorption and the TEM images, the emission bands at 408 nm and 503 nm are attributed to ZnO clusters encapsulated into the pores of the zeolites and ZnO nanocrystals on the surface of the zeolites, respectively. Upon further increasing the loading, t the component A decreases, and the center peak shifts from 404 to 422 nm. Moreover, the emission bands are very broad and have a large Stoke-shift compared to adsorption bands, which indicate the strong electron–phonon interaction between ZnO clusters and zeolites lattice.

Fig. 6 shows the emission spectra of the ZnO/L composites under the excitation of 325 nm. In the zeolite L, a broad band centering at about 485 nm appears and shifts to the red compared to the emission excited by 266 nm. These two bands may originate from the same kind of defect centers. According to the literature, the photoluminescence related to Si–O–Si was in the region of 300–550 nm [22]. The emission band centered at about 485 nm may also emanate from oxygen vacancies originating from Si–O–Si chemical bond. In the ZnO/L composites with 5 and 10 wt% ZnO loading, there exist two emission bands, a narrower band locating at 380 nm and a broader band centering at 500 nm. The former band is assigned to the recombination of ZnO excitons [23]. The latter band consists of the emission of the zeolite L, ZnO clusters inside the pores and the nanoparticles on the surface zeolite. As the

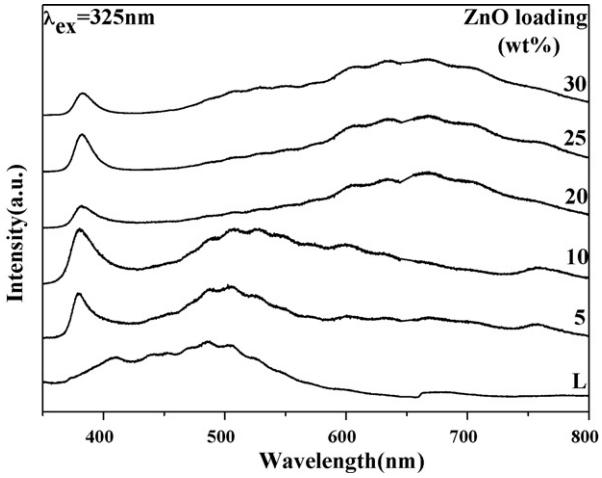

Fig. 6. Emission spectra of ZnO/L with different ZnO loadings ($\lambda_{ex} = 325$ nm).

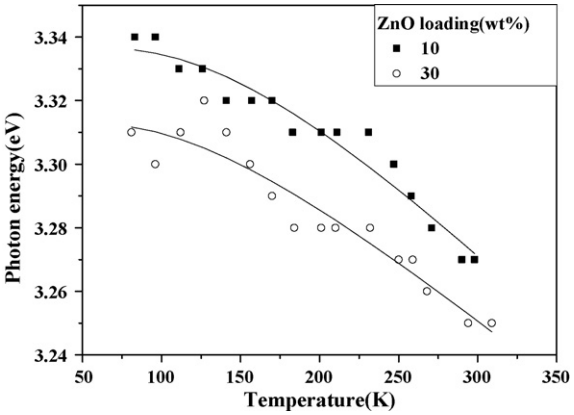

Fig. 7. The evolution of peak energy of the exciton emission as a function of temperature for the samples b and e. The scattered dots are the experimental data and solid lines are fitting functions (λ_{ex} = 325 nm).

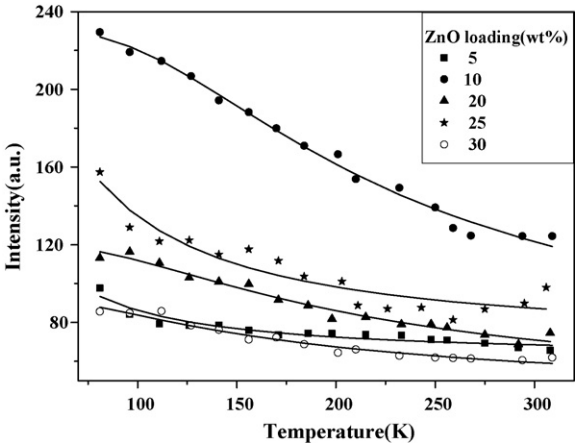

Fig. 8. The evolution of the integral intensity of the exciton peak as a function of temperature for the samples a, b, c, d and e. The scattered dots are the experimental data and solid lines are fitting functions (λ_{ex} = 325 nm).

ZnO loading is above 20 wt%, beside the exciton emission at 380 nm, a broad band centering at 665 nm emerges. This band is attributed to the defect emissions originating from macrocrystalline ZnO formed on the external surface of zeolite. This is consistent with the results from UV–vis absorption spectra and the TEM images.

3.3. Temperature dependence of photoluminescence

The emission spectra in different ZnO/L composites were measured at various temperatures under the 325 nm excitation. As a typical case, the energies of the exciton emissions for the samples with 10 and 30 wt% ZnO loadings were plotted as a function of temperature, as shown in Fig. 7. It can be seen that for the both samples, the transition energies decrease with the increasing temperature. The experimental results in the other samples are similar. Considering the exciton–photon interaction, the exciton energy as a function of temperature obeys the Bose–Einstein relation [24]:

$$E(T) = E_0 - \frac{A}{\exp(\Theta_E/T) - 1} \quad (2)$$

where E_0 is the transition energy of excitons at 0 K, A is the proportional coefficient, Θ_E is the Einstein characteristic temperature and T is the absolute temperature. The experimental data in all samples can be well fitted by Eq. (2) and the fitting parameters were listed in Table 2. It can be seen that the obtained values of A decrease with increasing ZnO loadings, that is, that exciton–phonon interaction is weaker in higher ZnO loading. This also demonstrates that the amount of the ZnO loading significantly affects the exciton–phonon interaction between the ZnO clusters and the zeolite host. The similar phenomena have been observed for CdS clusters inside zeolite [25]. It is possible that with decreasing the size of ZnO clusters, the non-radiative relaxation rate increases, the probability of inelastic collision between electrons and ZnO clusters increases, which results in the enhancement of the interaction of electron–phonon coupling.

Fig. 8 shows the temperature dependence of the emission intensity of excitons. It can be seen that the exciton intensity decreases with elevating temperature. In Fig. 8, the temperature-dependent intensity was fitted by the well-known thermal activation function [26]:

$$I(T) = \frac{I_0}{1 + \alpha \exp(-E_A/(k_B T))} \quad (3)$$

where I_0 is the emission intensity at 0 K, α is the proportional coefficient, E_A is the thermal activation energy, k_B is the Boltzmann's constant and T is the absolute temperature. The fitting parameters of all samples are listed in Table 2, which indicates that the thermal activation energy for the photoluminescence of 10 wt% ZnO/L is the largest and 5 wt% ZnO/L is the smallest among all the samples.

Fig. 9 shows the dependence of the emission intensity of the defects as a function of temperature. It can be seen that the emission intensity of the defects decreases with increasing temperature for all samples. The temperature-dependent intensity was also well fitted by Eq. (3). The fitting parameters for all samples are displayed in Table 2. It can be seen that E_A is larger in the sample of 25 wt% ZnO/L due to a large number of long-lived defect states involved in the sample of ZnO/L, as would be discussed by luminescence dynamics. The long-lived defect states should have smaller non-radiative relaxation rate and larger thermal activation rate than those of the short-lived defect states.

3.4. Luminescence dynamics

The fluorescent dynamics of ZnO clusters and the defects are obtained and listed in Table 3. Under the excitation of 260 nm, the

Table 2
The parameters of the exciton emission and the deep-level emission of ZnO/L with different ZnO loadings (λ_{ex} = 325 nm)

ZnO/L with different ZnO loading (wt%)	Peak energy of exciton			Intensity of exciton			Intensity of deep-level		
	E_0 (ev)	A	Θ_E (K)	I_0	α	E_A (meV)	I_0	α	E_A (meV)
5	3.31	0.24	469.9	715	10.8	3.3	1030	2.9	24.49
10	3.33	0.25	466.3	231	3.9	38.2	1323	3.9	23.71
20	3.31	0.21	463.8	121	2.1	28.7	839.5	3.6	36.97
25	3.32	0.15	360.7	293	3.3	9.0	3360	20.2	70
30	3.31	0.17	395.2	94	1.3	20.2	2592	5.1	48.89

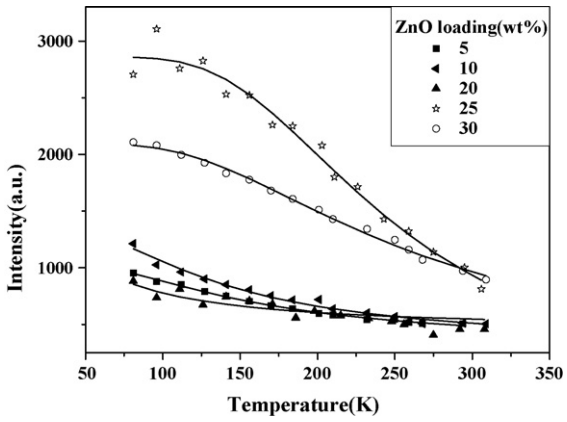

Fig. 9. The evolution of the integral intensity of the defects as a function of temperature for the samples a, b, c, d and e. The scattered dots are the experimental data and solid lines are fitting functions (λ_{ex} = 325 nm).

Table 3
Lifetimes of ZnO/L with different ZnO loadings (λ_{ex} = 260 nm)

ZnO/L with different ZnO loading (wt%)	λ = 404–422 nm, τ (ps)	λ = 518 nm, τ (ps)	λ = 630 nm τ (ps)
5	530	230	290
10	350	250	320
20	440	250	300
25	310	310	360
30	140	390	530

fluorescent lifetimes for ZnO clusters and the defects decays obey the single exponential rule. With increasing ZnO loading, the lifetimes of ZnO clusters vary from 530 to 140 ps and the lifetimes of defects increase. The lifetime is related to the dispersion amount of ZnO clusters in zeolite. Upon further increasing ZnO loadings, more macrocrystalline ZnO form on the external surface of zeolite L and fewer amounts of ZnO clusters disperse inside of zeolite. There are more defect states in the samples with higher ZnO loadings than those with lower ZnO loadings. Therefore, the lifetimes of ZnO clusters decrease and the lifetimes of defects increase with increasing ZnO loading.

4. Conclusions

In this paper, different amounts of ZnO clusters were introduced into the pores of microporous zeolites L by the incipient wetness impregnation method. The XRD, TEM, N_2 absorption, UV–vis, and PL spectra demonstrate that a small amount of sub-nanometric ZnO clusters can be encapsulated into the pores of zeolite. Some macrocrystalline ZnO cover the external surface of zeolite at high ZnO loading. The sub-nanometric ZnO clusters display significantly different optical properties from macrocrystalline ZnO mainly due to QSE. The absorption edge shows blue-shift below 255 nm and the blue luminescence band centers at 404–422 nm. The systemical study on temperature dependence of luminescence of the ZnO clusters indicate that the exciton–phonon interaction between the ZnO clusters and the zeolite host were significantly affected by the amount of the ZnO loading. Moreover, ZnO clusters and the defects related to the macrocrystalline ZnO exhibit picosecond scale emission lifetime at room temperature. The present findings may lead to potential applications in optoelectronics and help to design the light-emitting systems and other optical devices.

Acknowledgements

The work was financially supported by the Nation Natural Science Foundation of China (Grant Nos. 10704073, 50772042 and 10504030) and the 863 Project of China (Grant No. 2007AA03Z314).

References

[1] W. Park, J.S. King, C.W. Neff, C. Liddell, C. Summers, J. Phys. Status Solidi 229 (2002) 949–960.
[2] G. Hörner, P. Johne, R. Künneth, G. Twardzik, H. Roth, T. Clark, H. Kirsch, Chem.-Eur. J. 5 (1999) 208–217.
[3] M. Gaetzel, Platinum Met. Rev. 38 (1994) 151–159.
[4] Y.F. Chen, D.M. Bagnall, H. Koh, K. Park, K. Hiraga, Z. Zhu, T. Yao, J. Appl. Phys. 84 (1998) 3912–3918.
[5] W.Y. Liang, A.D. Yoffe, Phys. Rev. Lett. 20 (1968) 59–62.
[6] D.C. Reynolds, D.C. Look, B. Jogai, C.W. Litton, G. Cantwell, W.C. Harsch, Phys. Rev. B 60 (1999) 2340–2344.
[7] D.C. Look, Mater. Sci. Eng. B 80 (2001) 383–387.
[8] L.E. Brus, J. Chem. Phys. 80 (1984) 4403–4409.
[9] A. Henglein, Chem. Rev. 89 (1989) 1861–1873.
[10] R. Reisfeld, J. Alloys Compd. 341 (2002) 56–61.
[11] R. Viswanatha, S. Sapra, B. Satpati, P.V. Satyam, B.N. Dev, D.D. Sarma, J. Mater. Chem. 14 (2004) 661–668.
[12] T. Matsumoto, J. Suzuki, M. Ohnuma, Y. Kanemitsu, Y. Masumoto, Phys. Rev. B 63 (2001) 195322–195326.
[13] H. Xia, F. Tang, J. Phys. Chem. B 107 (2003) 9175–9178.
[14] X. Zhao, G. Lu, G.J. Millar, J. Porous Mater. 3 (1996) 61–66.
[15] T. Türk, F. Sabin, A. Vogler, Mater. Res. Bull. 27 (1992) 1003–1008.
[16] J. Chen, Z.C. Feng, P.L. Ying, C. Li, J. Phys. Chem. B 108 (2004) 12669–12676.
[17] O. Larlus, V.P. Valtchev, Chem. Mater. 16 (2004) 3381–3389.
[18] B.C. Lippens, J.H. de Boer, J. Catal. 4 (1965) 319–323.
[19] Y.C. Xie, Y.Q. Tang, Adv. Catal. 37 (1990) 1–43.
[20] F.S. Xiao, W. Xu, S. Qiu, R. Xu, J. Mater. Chem. 4 (1994) 735–739.
[21] L.E. Brus, J. Phys. Chem. 90 (1986) 2555–2560.
[22] Y. Zhu, H. Wang, P.P. Ong, Solid State Commun. 116 (2000) 427–429.
[23] T.W. Kim, T. Kawazoe, S. Yamazaki, M. Ohtsu, T. Sekiguchi, Appl. Phys. Lett. 84 (2004) 3358–3360.
[24] A. Setoguchi, H. Nakanishi, Appl. Phys. Lett. 76 (2000) 1576–1578.
[25] Y. Wang, N. Herron, J. Phys. Chem. 92 (1988) 4988–4994.
[26] B.S. Li, Y.C. Liu, Z.Z. Zhi, D.Z. Shen, Y.M. Lu, J.Y. Zhang, X.W. Fan, J. Cryst. Growth 240 (2002) 479–483.